734 J. Med. Chem. 2010, 53, 734–744
DOI: 10.1021/jm901375r

Journal of Medicinal Chemistry Article

Synthesis and Biological Evaluation of Amidine, Guanidine, and Thiourea Derivatives of 2-Amino-(6-trifluoromethoxy)benzothiazole as Neuroprotective Agents Potentially Useful in Brain Diseases†

Maurizio Anzini,*,‡ Alessia Chelini,‡ Alessandra Mancini,‡ Andrea Cappelli,‡ Maria Frosini,§ Lorenzo Ricci,§ Massimo Valoti,§ Jacopo Magistretti,∥ Loretta Castelli,∥ Antonio Giordani,⊥ Francesco Makovec,⊥ and Salvatore Vomero‡

‡Dipartimento Farmaco Chimico Tecnologico and European Research Centre for Drug Discovery and Development, Università di Siena, Via A. Moro, 53100 Siena, Italy, §Dipartimento di Neuroscienze, Sezione di Farmacologia, Fisiologia e Tossicologia, Università di Siena, Via A. Moro, 53100 Siena, Italy, ∥Dipartimento di Fisiologia, Sezione di Fisiologia Generale, Università di Pavia, Via Forlanini 6, 27100 Pavia, Italy, and ⊥Rottapharm SpA, Via Valosa di Sopra 7, 20052 Monza, Italy

Received September 29, 2009

A series of amidine, thiourea, and guanidine derivatives of 2-amino-6-(trifluoromethoxy)benzothiazole termed **2**, **3**, and **4**, respectively, and structurally related to riluzole, a neuroprotective drug in many animal models of brain disease, have been synthesized. The biological activity of compounds **2a**−**e**, **3a**−**f**, and **4a,b** was preliminarily tested by means of an in vitro protocol of ischemia/reperfusion injury. The results demonstrated that **2c** and **3a**−**d** significantly attenuated neuronal injury. Selected for testing of their antioxidant properties, compounds **3a**−**d** were shown to be endowed with a direct ROS scavenging activity. Compounds **3b** and **3d** were also evaluated for their activity on voltage-dependent Na^+ and Ca^{2+} currents in neurons from rat piriform cortex. At 50 μM, compound **3b** inhibited the transient Na^+ current to a much smaller extent than riluzole, whereas **3d** was almost completely ineffective.

Introduction

Excitatory amino acids (EAAs)[a] are neurotransmitters that play an important role in the development of both chronic neurodegenerative disorders like Alzheimer's (AD) and Parkinson's (PD) diseases as well as amyotrophic lateral sclerosis (ALS), and acute conditions such as brain ischemia and trauma.[1] Indeed, "excitotoxicity" is a term coined to describe an excessive release of glutamate, and a subsequent overactivation of excitatory amino acid receptors (NMDA, AMPA, and kainate). Glutamate-induced depolarization due to AMPA receptor activation is an early step in excitotoxicity and leads to Ca^{2+} influx through voltage-gated calcium channels and an intracellular Ca^{2+} concentration increase, subsequently amplified by release of Ca^{2+} from intracellular stores. Depolarization also promotes activation of voltage-dependent Na^+ channels, which, if uncontrolled, may cause the intracellular Na^+ concentration to abnormally increase.[2] This process can lead to osmotic swelling of the neuron as Cl^- passively enters the cell and is followed by the entry of water. Another consequence of depolarization is the release of the "Mg^{2+} block" from NMDA receptors, which allows them to generate a net ion flux in the presence of glutamate. Once activated, NMDA channels allow Ca^{2+} to flow into the neuron, which further increases the Ca^{2+} load to neuronal cytoplasm. An excessive $[Ca^{2+}]_i$ increase triggers a number of intracellular events which may eventually lead to cell damage or death. Among such Ca^{2+}-dependent responses are production of nitric oxide (NO) by neuronal nitric oxide synthase (*n*NOS)[3] and release of superoxide anion from mitochondria.[4] NO and superoxide then combine to form the highly reactive species peroxynitrite, which results in further Ca^{2+} influx and production of oxygen and nitrogen free radicals.

Each step of the excitotoxic cascade might be an attractive target for the development of neuroprotective agents potentially useful for treating many chronic and acute brain disorders.

Riluzole (**1**) or 2-amino-6-(trifluoromethoxy)benzothiazole (Chart 1) possesses neuroprotective effects in animal models of PD,[5] Huntington's disease,[6] and cerebral ischemia,[7] and it is currently the only drug that has proven to be able to modify the course of the disease[8−10] and is approved for the treatment of ALS. Riluzole conducts multiple molecular actions in vitro, among which those that have been documented to occur at physiologically realistic drug concentrations, and are therefore most likely to be clinically relevant, are inhibition of voltage-gated sodium channels,[11−14] which can lead to reduced neurotransmitter release, noncompetitive inhibition of NMDA receptors,[15,16] inhibition of glutamate release,[17] and enhanced astrocytic uptake of extracellular glutamate.[18]

On the basis of animal models of excitotoxicity and injury, many neuroprotective agents studied so far target a specific pathway of the excitotoxic cascade. On the other hand, animal

†In memory of Nello Manganelli, who struggled with amyotrophic lateral sclerosis and was the major inspirator for this work.

*To whom correspondence should be addressed. Phone: +39 (0)577 234173. Fax: +39 (0)577 234333. E-mail: anzini@unisi.it.

[a] Abbreviations: AD, Alzheimer's disease; PD, Parkinson's disease; ALS, amyotrophic lateral sclerosis; NMDA, *N*-methyl-D-aspartate; AMPA, α-amino-3-hydroxyl-5-methyl-4-isoxazolepropionate; L-NAME, nitro-L-arginine methyl ester; NO, nitric oxide; *n*NOS, neuronal nitric oxide synthase; LDH, lactate dehydrogenase; aCSF, artificial cerebrospinal fluid; OGD, oxygen/glucose deprivation; HVA, high-voltage-activated currents; ABTS, 2,2′-azinobis(3-ethylbenzthiazoline-6-sulfonic acid); sem, standard error of the mean.

 Published on Web 12/01/2009

Chart 1. Title and Reference Compounds

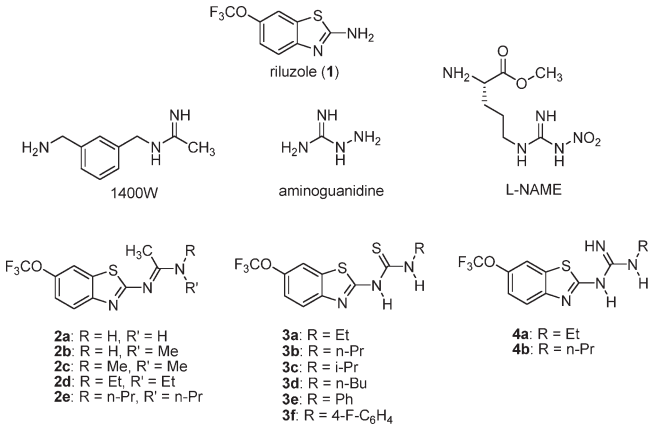

studies have shown that combination therapies have synergistic effects.[19] Therefore, it might be fruitful to explore novel treatments based on molecules endowed with multiple mechanisms of action. This study was intended to develop novel neuroprotective agents interfering with different biochemical steps of the pathways which lead to neuronal injury, to prevent or minimize tissue damage.

The synthesis of compounds **2**, **3**, and **4** (see Chart 1) closely related to riluzole (**1**) was thus performed.

In particular, we designed amidine and guanidine derivatives **2** and **4**, respectively (Chart 1), with the aim of conjugating the neuroprotective effects of riluzole with the neuroprotective and anti-inflammatory activity of 1400W,[20] and the NOS-inhibiting properties of aminoguanidine[21] and L-NAME[22] (Chart 1). Thiourea derivatives **3** (Chart 1) have been synthesized because many thioureas were found to be potent free radical scavengers able to prevent oxidative damage.[23]

The title compounds were tested for their ability to counteract the glutamatergic excitotoxic cascade by means of an in vitro model of cerebral ischemia, and their effects were compared to those of riluzole as the reference drug. In particular, the degree of neuroprotection afforded by compounds **2a**−**e**, **3a**−**f**, and **4a,b** was assessed in rat cortical brain slices subjected to oxygen/glucose deprivation (OGD) and reperfusion. Tissue damage and protection were assessed by measuring the release of glutamate and lactate dehydrogenase (LDH), the latter taken as an index of overall cellular injury. Moreover, compounds **3b** and **3d** were selected and tested with respect to their activity on voltage-dependent Na^+ and Ca^{2+} currents in neurons from rat piriform cortex by means of whole-cell, patch-clamp recordings: indeed, inhibition of voltage-gated Na^+ channels is an important mechanism of riluzole neuroprotective action, and excessive Ca^{2+} influx through ion channels is a crucial step in glutamate release and excitotoxicity. The ability of guanidine derivative **2c** to inhibit *n*NOS in vitro was also tested. Finally, to obtain a direct evidence that thiourea derivatives have a ROS scavenging capacity in vitro, the total equivalent antioxidant capacity (TEAC assay)[24] of compounds **3a**−**d** with respect to that of Trolox, a water-soluble vitamin E analogue, was measured.

Chemistry

2-Amino-6-(trifluoromethoxy)benzothiazole (**1**) was prepared via a one-pot procedure based on the condensation of 4-(trifluorometoxy)aniline with 1 molar equiv of ammonium thiocyanate and benzyltrimethylammonium tribromide in

Scheme 1[a]

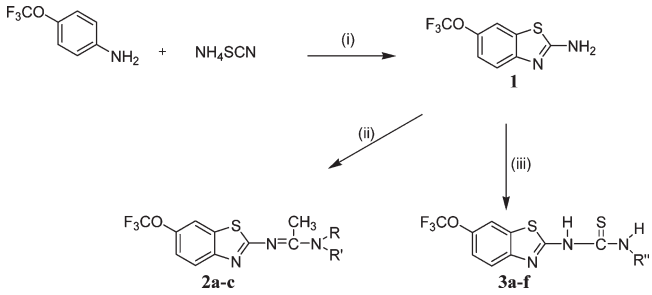

[a] Reagents and conditions: (i) NH_4SCN, $PhCH_2NMe_3Br_3$, CH_3CN, room temperature, 24 h; (ii) $POCl_3$, CH_3CONRR', dry toluene, reflux, 1−7 h; (iii) RNCS, Et_3N, dry toluene, reflux, 25−54 h.

Scheme 2[a]

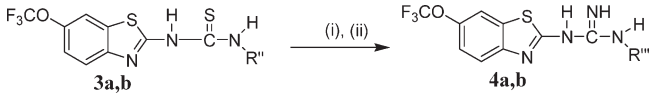

[a] Reagents and conditions: (i) CH_3I, acetone, 25 °C, 60 h; (ii) NH_3(g), 20 min, EtOH, room temperature, 20 h.

CH_3CN as previously described[25] but in higher yields (80%) (Scheme 1). The reaction of compound **1** with the appropriate acetamide in the presence of $POCl_3$ in dry toluene led to the formation of the desired acetamidines **2a**−**c**. To prevent degradation and to enhance their stability, we converted compounds **1** and **2a**−**c** to the corresponding hydrochloride salts. As for the thiourea derivatives, synthesized as shown in Scheme 1, compound **1** was treated with the corresponding proper isothiocyanate upon addition of triethylamine to give desired products **3a**−**f**.[26] In this case, a high-boiling point solvent such as toluene guaranteed good yields.

Finally, guanidines **4a,b** were obtained by reaction of the corresponding thioureas (**3a,b**) with methyl iodide in acetone followed by treatment with anhydrous ammonia in ethanol[27] (Scheme 2).

Results and Discussion

Neuroprotective Effects of the New Compounds. Neuroprotection exerted by compounds **2a**−**e**, **3a**−**f**, and **4a,b** was evaluated in an in vitro model that mimics neuronal ischemia and excitotoxicity, namely rat cortical brain slices subjected to OGD and reperfusion. The compounds were added to the reoxygenation buffer in a concentration range of 0.001−100 μM, and their effects were compared with those of riluzole, taken as the reference drug. As shown in Table 1, riluzole significantly reduced the levels of OGD- and reoxygenation-induced LDH and glutamate release. Its effects, however, followed a "U-shaped" concentration−response curve typical of a hormetic response, with an "efficacy window" between 0.1 and 25 μM (Figure 1).

The most effective riluzole concentrations turned out to be 1−25 μM, which were capable of decreasing the release of glutamate from 0.65 ± 0.04 nmol/mg of wet tissue (OGD) to 0.27 ± 0.02 nmol/mg of tissue ($P < 0.01$; $n = 9$) and that of LDH from 18.0 ± 0.9 units/mg of protein (OGD) to 5.38 ± 1.01 units/mg of protein ($P < 0.01$; $n = 11$). Some of the tested compounds were effective in reducing OGD-induced LDH and glutamate release, although with different potencies. In particular, **2c** and **3b** were the most interesting compounds (Figure 1, panels B and D, respectively).

Table 1. Effects of Riluzole and Compounds **2c** and **3a−d** on OGD- and Reperfusion-Induced Release of Glutamate (GLU) and Lactate Dehydrogenase (LDH) in Rat Cortical Brain Slices

	GLU release		LDH release	
compound	efficacy window[a] (μM)	MEC[b] (% ± sem)[c]	efficacy window[a] (μM)	MEC[b] (% ± sem)[c]
riluzole	1−25	1−10 (100.0 ± 5.1)	0.1−100	10−25 (100.0 ± 4.5)
2c	0.1−10	0.1 (100.0 ± 4.3)	0.1−25	0.1 (56.9 ± 2.8)
3a	1	1 (80.1 ± 4.1)	0.1−10	0.1 (73.1 ± 3.5)
3b	0.01−10	0.01 (94.2 ± 3.8)	0.01	0.01 (60.9 ± 2.9)
3c	0.01−1	0.1 (80.3 ± 3.9)	0.01	0.01 (50.0 ± 2.7)
3d	0.01−1	1 (100.0 ± 3.2)	0.01	0.01 (32.0 ± 2.2)

[a] The efficacy windows represent the interval of concentrations at which a significant reduction of OGD-induced GLU and LDH release was observed. [b] MEC (minimal effective concentration) is the micromolar concentration at which the highest level of reduction was observed. [c] The value between parentheses represents the percent of reversion exerted at such concentration; 100% is taken as the return to basal values (control).

Indeed, in the concentration range of 0.1−25 μM (**2c**) or 0.001−0.1 μM (**3b**), they fully antagonized OGD-induced glutamate release while partially preventing that of LDH. Considering that several pathways leading to cell death are activated in cerebral ischemia,[28] these results suggest that compounds **2c** and **3b** interfere selectively with the crucial steps promoting glutamate release and not with those leading to LDH leakage.

Compound **3a** reduced LDH efflux caused by OGD and reperfusion by ~70% ($P < 0.01$) in the concentration range between 0.1 and 10 μM, whereas it was less efficient against glutamate release (Figure 1C). Finally, **3c** and **3d** completely reversed glutamate release in the concentration range between 0.01 and 1 μM but were largely ineffective toward LDH efflux (panels E and F of Figure 1, respectively).

On the other hand, compounds **2a,b,d,e**, **3e,f**, and **4a,b** were not able to significantly antagonize OGD-induced glutamate and LDH release, when added during a 90 min reperfusion phase. Moreover, concentrations of such compounds between 50 and 100 μM promoted a significant glutamate release (data not shown).

***n*NOS Inhibition and Antioxidant Activity.** To gain insight into the mechanism of action of the new compounds, some potential pharmacological effects expected on the basis of the molecules' chemical design were then evaluated. In particular, the ability of amidine derivative **2c** to inhibit *n*NOS in vitro was also assessed by using partially purified rat brain enzyme.[29] *n*NOS activity was determined by measuring the conversion of oxyhemoglobin to methemoglobin by NO at a λ of 401 nm.[30] However, our results indicate that **2c** did not significantly inhibit *n*NOS activity (data not shown), suggesting that its neuroprotective activity was not related to this effect.

Then, the total antioxidant activity of compounds **3a−d** was evaluated by means of the ABTS cation decolorization assay.[24] This method is based on the ability of antioxidant molecules to quench the stable radical cation, $ABTS^{\bullet+}$, a blue-green chromophore with characteristic absorption at 734 nm. The concentration of antioxidant giving the same percent $ABTS^{\bullet+}$ absorbance inhibition of 1 mM Trolox was calculated (Trolox equivalent antioxidant activity, TEAC). A TEAC value close to 1.00 indicated that the antioxidant had a scavenging activity similar to that of Trolox.

All the tested compounds exhibited a TEAC value ranging between 0.98 and 0.50 [0.88 ± 0.17 for **3a**, 0.50 ± 0.05 for **3b**, 0.64 ± 0.02 for **3c**, and 0.98 ± 0.14 for **3d** (Table 2)], whereas riluzole was ineffective. Interestingly, the antioxidant ebselen, which protects neuronal cells against oxidative stress by acting at multiple steps,[31] had a TEAC value much lower than those of the compounds mentioned above. These results strongly indicate that compounds **3a−d** can directly scavenge ROS and suggest that this activity might contribute to their neuroprotective effects.

Taken together, the results reported above indicate that compounds **2c** and **3a−d** displayed interesting neuroprotective properties but different potencies. Their global effects, however, are inferior to those of riluzole, as indicated by the biochemical assay of LDH release taken as an index of overall cellular injury in this study. Indeed, none of them was able to completely antagonize the efflux of the intracellular enzyme. In the light of these considerations, it could be worth further characterizing the molecular mechanism(s) underlying the effects of compounds **2c** and **3a−d** toward ischemia/reperfusion injury as well as the receptor(s) potentially involved.

Effects of Compounds 3b and 3d on Voltage-Dependent Na^+ and Ca^{2+} Currents. Inhibition of voltage-dependent Na^+ currents through a mechanism involving stabilization of the Na^+ channel's inactivated state is a well-established effect of riluzole[11−14] and is believed to be an important basis of this drug's neuroprotective action. Moreover, in peripheral sensory neurons riluzole also exerts an inhibitory effect on high-voltage-activated (HVA) Ca^{2+} currents.[32] Indeed, inhibition of voltage-dependent Ca^{2+} influx under conditions of metabolic distress and depolarization could contribute to reducing the level of glutamate release, thus partly justifying the effects of riluzole and compounds like **3b** and **3d**. Therefore, **3b** and **3d** were tested to evaluate their activity on neuronal voltage-dependent Na^+ and Ca^{2+} currents and compare it with that of riluzole.

Patch-clamp[33] recordings of voltage-dependent Na^+ currents were performed using neurons of rat piriform cortex layer II in brain slices as an experimental model (see the Experimental Section for all details of the patch-clamp experiments). Differently from acutely dissociated neurons (see below), this preparation allowed for optimal Na^+ current stability, as required to evaluate the activity of the drugs examined. The transient Na^+ current (I_{NaT}) was studied by applying a current−voltage (I/V) protocol consisting of 19 ms depolarizing step pulses at −75 to 20 mV in 5 mV increments, starting from a holding potential of −80 mV (not shown). During drug application, the I_{NaT} amplitude was also monitored by repetitively commanding (once every 10 s) a single 19 ms step at −20 mV. Riluzole, **3b**, or **3d** was applied through the bath perfusion at 50 μM. After a saturating effect on the I_{NaT} amplitude was reached, the drug's effect was quantified by measuring I_{NaT} inhibition at a voltage level equal to the I/V peak plus 20 mV (Figure 2A), rather than at the peak itself, to minimize the consequences of space-clamp artifacts (see ref 34). Whereas 50 μM riluzole

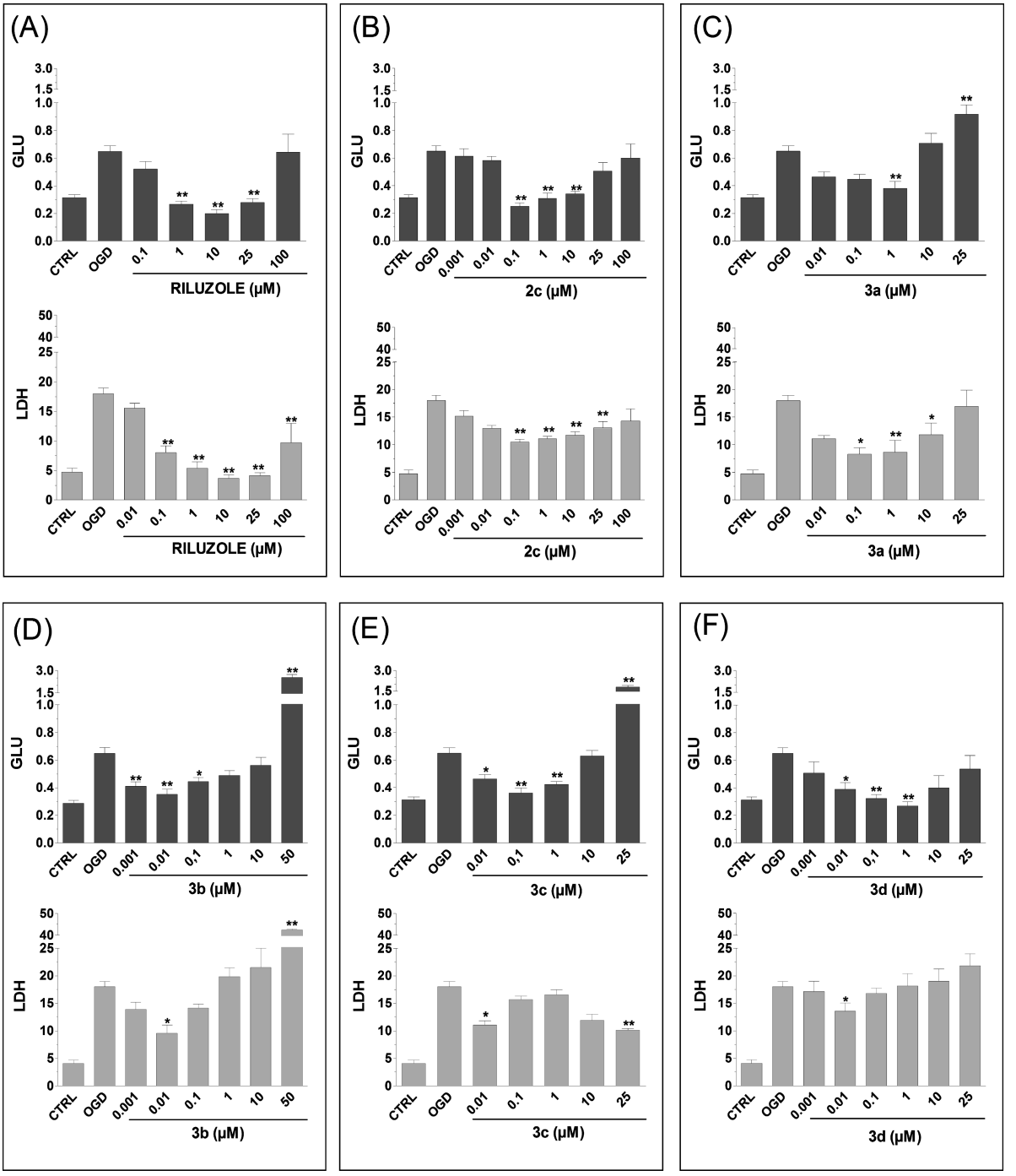

Figure 1. Effects of riluzole (A) and compounds **2c** (B), **3a** (C), **3b** (D), **3c** (E), and **3d** (F) on oxygen/glucose deprivation- and reoxygenation-induced release of GLU and LDH, in rat cortical slices. Drugs were added to reoxygenation buffer after OGD for 30 min. Data are means ± sem of at least four different experiments. Statistical analysis was performed by using ANOVA followed by a post hoc Dunnett test. One asterisk indicates $P < 0.05$, and two asterisks indicate $P < 0.01$ vs OGD.

Table 2. Relative Antioxidant Activities (TEAC)

compound	TEAC value[a]
Trolox	1.00 ± 0.00
ebselen[31]	0.32 ± 0.06
riluzole	not active
3a	0.88 ± 0.17
3b	0.50 ± 0.05
3c	0.64 ± 0.02
3d	0.98 ± 0.14

[a] Values are presented as means ± sem of at least three experiments.

reduced the I_{NaT} amplitude by more than 50%, **3b** and **3d** had much weaker effects (~15 and ~0% inhibition, respectively) (Figure 2B). The differences were statistically highly significant ($P < 0.001$ with respect to riluzole in both cases). Hence, the attachment of the 1-propylthioureidic group and, even more, the 1-butylthioureidic group to the amino group in position 2 of riluzole's benzothiazole ring causes a drastic decrease in the drug's potency in interacting with voltage-gated Na^+ channels. Therefore, the effects of **3b** and **3d** on voltage-dependent Na^+ currents were not further characterized.

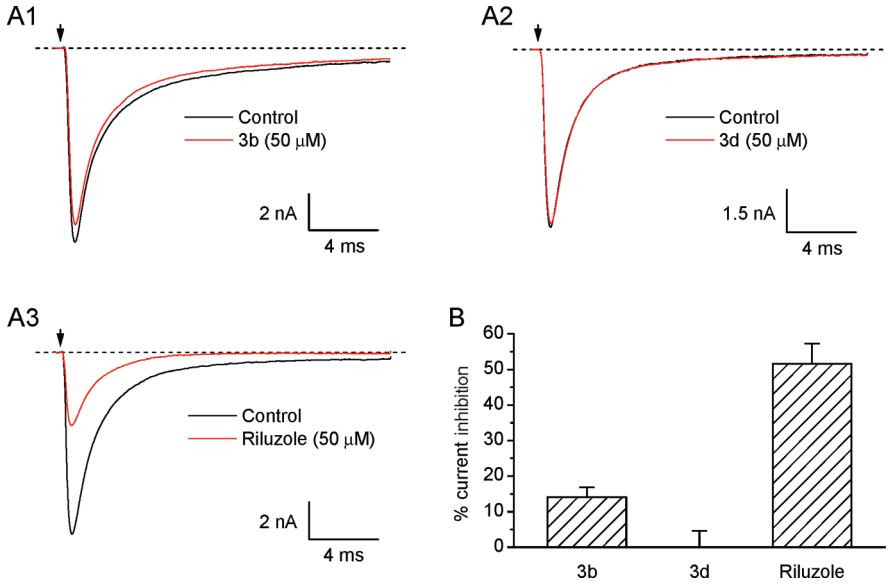

Figure 2. Inhibitory action of compounds **3b** and **3d** on the voltage-dependent, transient Na^+ current (I_{NaT}) in rat piriform cortex neurons. (A) I_{NaT} current tracings recorded in three different, representative neurons under control conditions and in the presence of 50 μM **3b** (A1), **3d** (A2), or riluzole (A3). The currents shown here were recorded at a test potential equal to the peak of the I/V relationship plus 20 mV (−5 or −10 mV). (B) Average values of I_{NaT} amplitude percent inhibition caused by 50 μM **3b** (n = 4), **3d** (n = 9), or riluzole (n = 6).

Voltage-dependent Ca^{2+} currents were studied in acutely dissociated neurons from rat piriform cortex layer II,[35] in which they proved to be highly stable and optimal clamp conditions could be achieved. Ba^{2+} was used instead of Ca^{2+} as the charge carrier, and Ba^{2+} currents (I_{Ba}) were recorded. High-voltage-activated (HVA) currents were elicited by commanding depolarizing step or ramp protocols starting from a conditioning potential of −60 mV. **3b** and **3d** were applied to the recorded neuron using a focal perfusion system.[35] Riluzole was also tested as a control. The effects of compounds **3b** and **3d** on HVA currents were monitored by repetitively commanding (once every 7 s) a voltage-clamp protocol consisting of a 40 ms depolarizing ramp from −60 to 30 mV, which returned an "instantaneous" I/V relationship for total HVA currents (see Figure 3B). This instantaneous I/V closely matched that obtained with standard step I/V protocols (see Figure 3B and the inset). Current amplitude was measured at the peak of the instantaneous I/V. Both drugs reduced HVA current amplitude in a concentration-dependent manner (Figure 3B). This inhibitory effect fully developed after drug perfusion for ~1 min (in Figure 3A, the horizontal bar indicates the time periods during which control solution and the various drug concentrations were perfused) and appeared to be largely irreversible after prolonged drug washout (not shown).

The percent HVA current inhibition as a function of drug concentration is illustrated in Figure 3C. Experimental data points were fitted with a Hill function of the form $y = 100 \times [D]^n/(IC_{50}{}^n + [D]^n)$, where [D] is the drug molar concentration and n is the Hill coefficient. Fitting parameters were as follows: IC_{50} = 112.9 μM, n = 0.58 (**3b**); IC_{50} = 24.1 μM, n = 0.82 (**3d**); IC_{50} = 34.2 μM, n = 0.82 (riluzole). It should be noted that both **3b** and **3d**, but not riluzole, tended to precipitate when added to the extracellular Ca^{2+} current recording solution at the highest concentrations employed (60 and 200 μM), thus yielding actual concentrations lower than nominal ones. This could explain the poor steepness of the dose−response curve observed especially for **3b**, in which case the Hill coefficient returned by fitting was as low as 0.58. The potency of the two drugs could therefore be somewhat underestimated in these experiments.

In dorsal-root-ganglion neurons, the inhibitory effect of riluzole on HVA currents was found to be voltage-independent.[32] Riluzole was also reported to accelerate the activation and deactivation kinetics of HVA currents, although, as far as deactivation is concerned, only at relatively positive potentials.[32] Therefore, the effects of **3d**, which appeared to be the more active compound with respect to HVA currents, were characterized in more depth and compared with those of the parental molecule by also analyzing HVA current voltage dependence and kinetics. The voltage dependence of HVA currents was studied by applying the I/V protocol illustrated in Figure 4 (panel A1). The I/V plots obtained in the presence of riluzole (n = 3; not shown) or **3d** (Figure 4B) were largely superimposable with those obtained under control conditions. The voltage dependence of HVA channel activation was further quantified by fitting I/V plots with a combination of a single Boltzmann function and the Goldman equation (see the Experimental Section, eq 1). Average values of the fitting parameters thus obtained are listed in Table 3. Both half-activation potential ($V_{1/2}$) and the slope factor (k) were not significantly different in the presence of riluzole or **3d** as compared to control. Therefore, neither riluzole nor **3d** significantly modifies the voltage dependence of activation of HVA Ca^{2+} channels in the central neurons studied here.

Riluzole and **3d** also had no consistent effect on HVA current activation speed, quantified by measuring the current rise time of 10−90% (RT_{10-90}) over the whole voltage range explored [n = 3 for riluzole, and n = 4 for **3d** (not shown)]. Instead, both drugs induced some significant modification of HVA current deactivation, although at relatively positive potentials only. This was revealed by the study of the decay kinetics of tail currents elicited upon repolarization (Figure 5A−C). As shown in Figure 5 (panels D and E1), **3d** (60 μM) significantly accelerated the "fast" deactivation time constant (τ_{d1}) at the most positive repolarization potential examined (−20 mV), but not at more negative voltages.

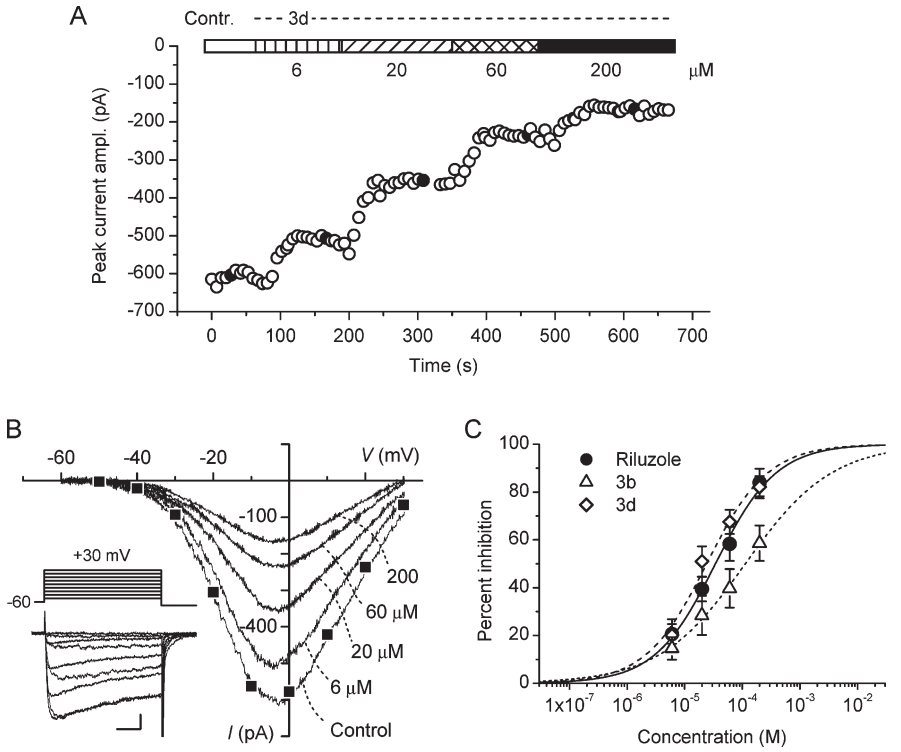

Figure 3. Inhibitory action of compounds **3b** and **3d** on high-voltage-activated Ca^{2+} currents in rat piriform cortex neurons. (A) Time course of the effects of increasing **3d** concentrations on the peak amplitude of total HVA currents in a representative neuron. HVA currents were evoked by ramp depolarizations (see the text). The filled circles correspond to the peak amplitudes of the representative current tracings shown in panel B. (B) Representative currents recorded in the same neuron of panel A under control conditions and in the presence of a steady inhibition by increasing **3d** concentrations. The inset shows the currents recorded in the same neuron by applying, under control conditions, a step I/V protocol (the voltage protocol is illustrated in the top part of the inset). Peak current amplitudes of these currents are indicated by the filled squares in the main panel. Calibration bars in the inset are for 10 ms and 100 pA. (C) Dose−response curve for the inhibitory effect exerted by **3b**, **3d**, and riluzole on the total HVA current peak amplitude. Smooth lines are fittings with Hill functions (see the text).

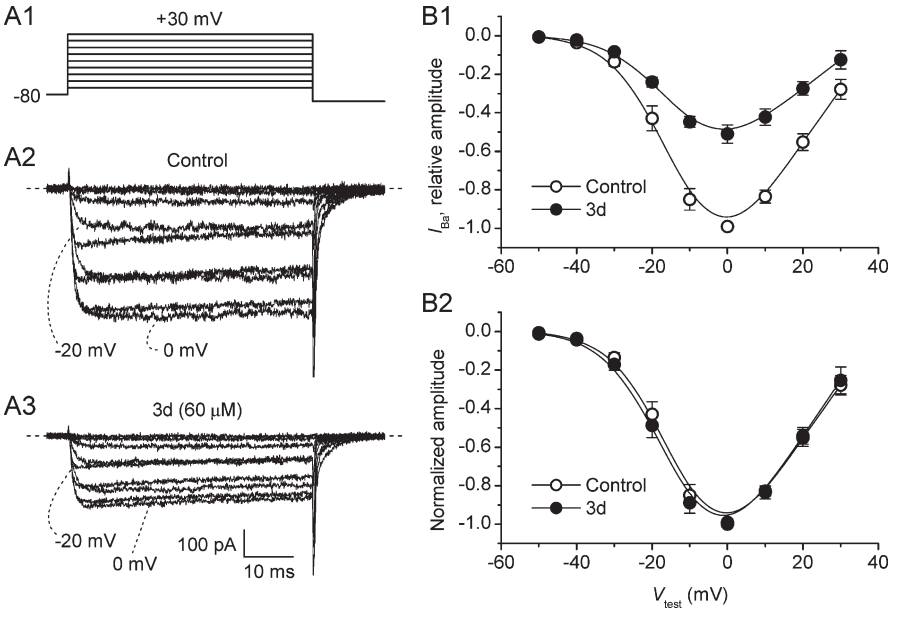

Figure 4. Compound **3d** does not modify the voltage dependence of activation of HVA Ba^{2+} currents. (A) Ba^{2+} currents evoked by a step I/V protocol (A1) in a representative neuron under control conditions (A2) and in the presence of 60 μM **3d** (A3). (B) Average I/V relationships of Ba^{2+} currents recorded, in response to the protocol illustrated in A1, in the absence and presence of 60 μM **3d**. In each cell, the peak current amplitude was measured at every test potential and then normalized for the maximal values observed under control conditions (normally at 0 mV). Current values thus normalized were then averaged among cells, and the resulting average plots are shown in panel B1. Peak current values were also normalized for the maximal values observed under each experimental condition (control, **3d**) and averaged among cells: the resulting average plots are shown in panel B2. Each data point is the average from five cells.

A similar effect was caused by riluzole (60 μM) (Figure 5, panel E2). Hence, **3d** modifies HVA Ca^{2+} channel deactivation kinetics in a manner similar to that of riluzole in the central neurons studied here.

Overall, our results indicate that compounds **3b** and **3d** do act on HVA Ca^{2+} channels, but at concentrations considerably higher than those required to antagonize OGD-induced glutamate and LDH release, and that their activity, if any, on voltage-gated Na^+ channels is much weaker than that of riluzole. This suggests that at the basis of the neuroprotective effects of these new compounds there are mechanisms probably independent of voltage-gated Na^+ and Ca^{2+} channels.

Table 3. Parameters of HVA Current Voltage Dependence of Activation under Control Conditions and in the Presence of Compound **3d** or Riluzole

	$V_{1/2}$ (mV)[a]	P^b	k (mV)[a]	P^b	n
control	-6.8 ± 2.0		7.9 ± 0.6		
riluzole (60 μM)	-6.5 ± 2.2	0.75	8.3 ± 0.5	0.16	3
control	-7.2 ± 1.8		7.5 ± 0.4		
3d (60 μM)	-7.5 ± 1.7	0.55	7.9 ± 0.6	0.17	5

[a] These parameters were returned by fitting the I/V relationships of HVA currents with a combination of the Boltzmann function and the Goldman equation (see the Experimental Section, eq 1). [b] Level of statistical significance of the differences observed between drug and control (t test for paired data).

Conclusions

A series of amidine, guanidine, and thiourea derivatives of 2-amino-6-(trifluoromethoxy)benzothiazole have been synthesized, and their ability to counteract the excitotoxic cascade has been evaluated. In an in vitro protocol of ischemia/reperfusion injury, some of them significantly attenuated neuronal injury in a concentration range between 0.1 and 25 μM. Furthermore, thioureas **3b** and **3d** were also tested to evaluate their activity on voltage-dependent Na^+ and Ca^{2+} currents in neurons from rat piriform cortex. At 50 μM, **3b** inhibited Na^+ currents to a much lesser extent than riluzole, whereas **3d** was almost inactive. Both compounds inhibited high-voltage-activated Ca^{2+} currents in a concentration-dependent manner, with an IC_{50} of 24.1 μM for **3d** and 112.9 μM

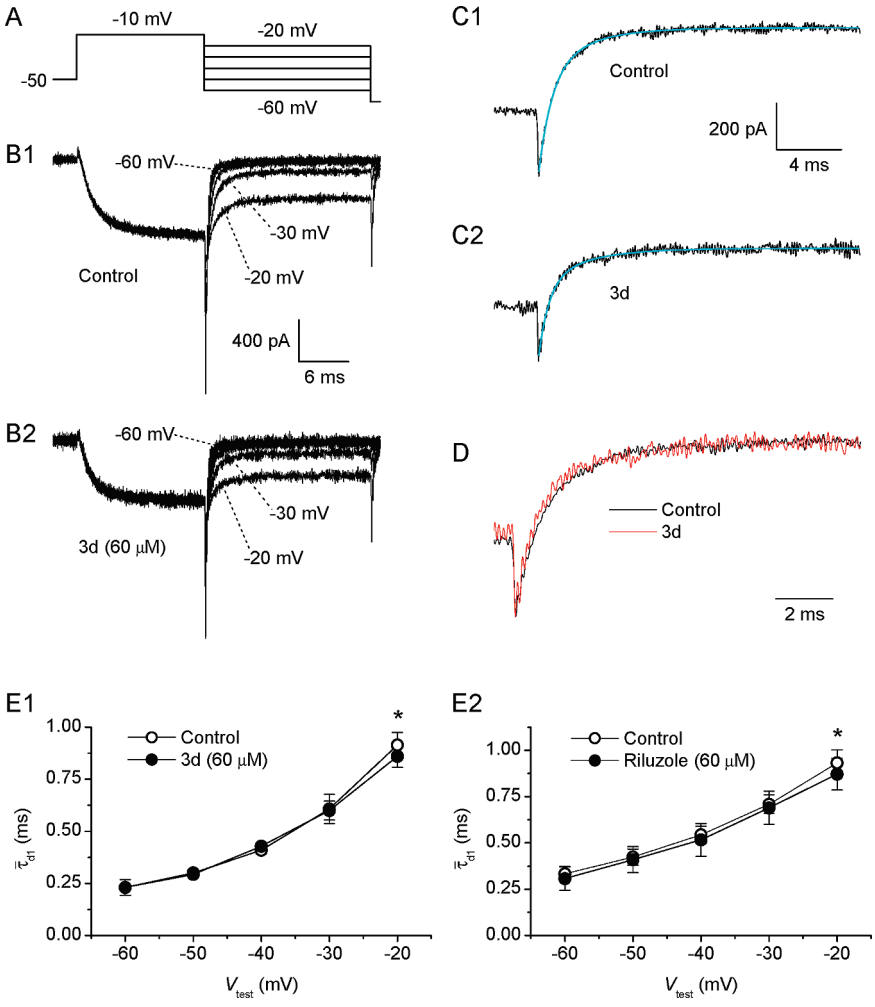

Figure 5. Effects of compound **3d** and riluzole on HVA I_{Ba} deactivation kinetics. (A and B) Voltage-clamp protocol applied to evoke tail currents upon repolarization (A) and Ba^{2+} currents thus recorded in a representative neuron under control conditions (B1) and in the presence of 60 μM **3d** (B2). (C) Detail of the tail currents recorded at the repolarization potential of -20 mV. The currents' decay phase has been fitted with a second-order exponential function (see the Experimental Section, eq 2) (blue lines). Fitting parameters are as follows: $A_1 = -406.8$ pA, $\tau_{d1} = 0.823$ ms, $A_2 = -206.8$ pA, $\tau_{d2} = 2.62$ ms, $C = -374.4$ pA (control); $A_1 = -308.0$ pA, $\tau_{d1} = 0.647$ ms, $A_2 = -152.5$ pA, $\tau_{d2} = 2.79$ ms, $C = -336.2$ pA (**3d**). (D) Further detail of tail currents shown in panel C, after zeroing of the offset level and normalization for peak amplitude. Note the slightly faster decay kinetics in the presence of **3d**. (E) Plot of the average, "weighted" fast deactivation time constant (τ_{d1}) (see the Experimental Section, eq 3, for details) as a function of repolarization potential, under control conditions and in the presence of 60 μM **3d** (E1) or riluzole (E2) ($n = 4$ in both cases). One asterisk indicates $P < 0.05$ (t test for paired data).

for **3b**. These observations strongly suggest that at the basis of neuroprotective effects of **3b** and **3d** are mechanisms that probably do not importantly involve voltage-gated Na^+ and Ca^{2+} channels.

Finally, compounds **3a**−**d** showed additional antioxidant properties, measured as Trolox equivalent activity, suggesting that they are also endowed with a direct ROS scavenging ability probably responsible for their ability to counteract ischemia-induced injury in vitro.

Further studies will be needed to characterize the neuroprotective effects of these compounds and to determine whether they could provide a basis for new therapeutic approaches to brain diseases.

Experimental Section

Chemistry. All chemicals used were of reagent grade. Yields refer to purified products and are not optimized. Melting points were determined in open capillaries on a Gallenkamp apparatus and are uncorrected. Microanalyses were conducted by means of a Perkin-Elmer 240C or a Perkin-Elmer Series II CHNS/O Analyzer 2400 to confirm the purity (≥95%) of the target compounds used in the biological testing. Merck silica gel 60 (230−400 mesh) was used for column chromatography. Merck TLC plates (silica gel 60 F_{254}) were used for TLC. ^{1}H NMR spectra were recorded with a Bruker AC 200 spectrometer in the indicated solvent (TMS as internal standard): the values of the chemical shifts (δ) are expressed in parts per million and the coupling constants (J) in hertz. Mass spectra were recorded on either a Varian Saturn 3 spectrometer or a ThermoFinnigan LCQ-deca instrument.

2-Amino-6-(trifluoromethoxy)benzothiazole (1). To a mixture of 4-trifluoromethoxyaniline (2.1 mmol) and ammonium thiocyanate (2.0 mmol) in CH_3CN (15 mL) was added benzyltrimethylammonium tribromide (2.0 mmol) at room temperature. The reaction mixture was stirred for 24 h, neutralized with aqueous $NaHCO_3$, and extracted with CH_2Cl_2. The combined organic layers were washed with water, dried over Na_2SO_4, filtered, and evaporated in vacuo. The crude material was purified by flash chromatography on silica gel eluting with a petroleum ether/ethyl acetate (1:1, v/v) mixture to give a solid that after recrystallization from *n*-hexane and dietyl ether gave light-yellow square platelets in 80% yield.

The analytical data, melting point, and ^{1}H NMR spectrum were consistent with those reported in the literature.[36]

2-Amino-6-(trifluoromethoxy)benzothiazole Hydrochloride. To a solution of compound **1** (1.3 mmol) in methanol (10 mL) was carefully added a concentrated 37% HCl solution (1 mL). The resulting solid was recrystallized from methanol to give white needles in quantitative yield. Crystals were filtered, washed with dry diethyl ether, and dried: mp 214−216 °C.

General Procedure for the Preparation of Acetamidine Derivatives (2a−e). To an ice-cooled solution of phosphorus oxychloride (0.85 mmol) in dry toluene (20 mL) was added the suitable amount of acetamide (0.47 mmol), and the mixture was stirred for 30 min at room temperature. At the end of the reaction, compound **1** (0.42 mmol) dissolved in dry toluene was added dropwise and the reaction mixture was refluxed for the proper time. The solution was then cooled, carefully poured into ice−water, and made alkaline with a 1 N NaOH solution. The organic layer was extracted with $CHCl_3$, washed to neutrality with water, dried over Na_2SO_4, filtered, and then evaporated in vacuo. The crude material was purified by flash chromatography on silica gel eluting with a petroleum ether/ethyl acetate (4:6, v/v) mixture, and the expected compound was transformed into the corresponding hydrochloride salt [as described for 2-amino-6-(trifluoromethoxy)benzothiazole hydrochloride] and then crystallized from the indicated solvent.

(i) *N*′-[6-(Trifluoromethoxy)benzothiazol-2-yl]acetamidine (2a). Reflux for 6 h: light-yellow solid (67% yield); ^{1}H NMR ($CDCl_3$) δ 2.35 (s, 3H), 5.62 (br s, 2H), 7.20 (m, 2H), 7.48 (d, 1H, J = 8.9); MS-ESI m/z 276 ($M + H^+$).

(ii) *N*′-[6-(Trifluoromethoxy)benzothiazol-2-yl]acetamidine Hydrochloride. White square platelets from a methanol/diethyl ether mixture: mp 202−206 °C.

(iii) *N*-Methyl-*N*′-[6-(trifluoromethoxy)benzothiazol-2-yl]acetamidine (2b). Reflux for 7 h: yellow solid (21% yield); ^{1}H NMR ($CDCl_3$) δ 2.21 (s, 3H), 3.11 (d, 3H, J = 5.1), 7.18 (d, 1H, J = 8.3), 7.58 (m, 2H), 10.68 (br s, 1H); MS-ESI m/z 290 ($M + H^+$).

(iv) *N*-Methyl-*N*′-[6-(trifluoromethoxy)benzothiazol-2-yl]acetamidine Hydrochloride. Light-yellow square platelets from methanol: mp 202 °C.

(v) *N*,*N*-Dimethyl-*N*′-[6-(trifluoromethoxy)benzothiazol-2-yl]-acetamidine (2c). Reflux for 1 h: light-yellow solid (34% yield); ^{1}H NMR ($CDCl_3$) δ 2.25 (s, 3H), 3.06 (s, 6H), 7.14 (d, 1H, J = 8.7), 7.48 (s, 1H), 7.61 (d, 1H, J = 8.8); MS-ESI m/z 304 ($M + H^+$).

(vi) *N*,*N*-Dimethyl-*N*′-[6-(trifluoromethoxy)benzothiazol-2-yl]-acetamidine Hydrochloride. Light-orange square platelets from methanol: mp 219−222 °C.

(vii) *N*,*N*-Diethyl-*N*′-[6-(trifluoromethoxy)benzothiazol-2-yl]-acetamidine (2d). Reflux for 3 h: light-yellow oil (58% yield); ^{1}H NMR ($CDCl_3$) δ 1.21 (t, J = 7.1, 6H), 2.31 (s, 3H), 3.49 (br s, 4H), 7.15 (d, J = 8.8, 1H), 7.49 (s, 1H), 7.63 (d, J = 8.8, 1H); MS-ESI m/z 332 ($M + H^+$).

(viii) *N*,*N*-Dipropyl-*N*′-[6-(trifluoromethoxy)benzothiazol-2-yl]-acetamidine (2e). Reflux for 3 h: yellow oil (52% yield); ^{1}H NMR ($CDCl_3$) δ 0.92 (t, J = 7.2, 6H), 1.66 (m, 4H), 2.30 (s, 3H), 3.36 (br d, 4H), 7.15 (d, J = 9.0, 1H), 7.49 (s, 1H), 7.63 (d, J = 8.9, 1H); MS-ESI m/z 360 ($M + H^+$).

General Procedure for the Preparation of Thiourea Derivatives (3a−f). To a solution of **1** (2.7 mmol) in dry toluene (20 mL) were added triethylamine (0.43 mmol) and the suitable amount of isothiocyanate (3.78 mmol). The reaction mixture was refluxed for the suitable time and then cooled. The solvent was removed under reduced pressure, and the residue, diluted with CH_2Cl_2, was washed with water, dried over Na_2SO_4, filtered, and evaporated under reduced pressure. The resulting residue was purified by flash chromatography with a petroleum ether/ethyl acetate (65:35, v/v) mixture to give a solid that after recrystallization from ethyl acetate and diethyl ether afforded the required product.

(i) 1-Ethyl-3-[6-(trifluoromethoxy)benzothiazol-2-yl]thiourea (3a). Reflux for 30 h: light-yellow needles (36% yield); mp 199−200 °C; ^{1}H NMR (DMSO-d_6) δ 1.17 (t, 3H, J = 7.20), 3.55 (m, 2H), 7.37 (d, 1H, J = 8.4), 7.70 (d, 1H, J = 8.7), 8.02 (s, 1H), 9.54 (br s, 2H); MS-ESI m/z 320 ($M - H^+$).

(ii) 1-Propyl-3-[6-(trifluoromethoxy)benzothiazol-2-yl]thiourea (3b). Reflux for 25 h: yellow needles (40% yield); mp 226−228 °C; ^{1}H NMR (DMSO-d_6) δ 0.90 (t, 3H, J = 7.3), 1.57 (m, 2H), 3.48 (m, 2H), 7.35 (d, 1H, J = 8.5), 7.79 (d, 1H, J = 44.6), 8.01 (s, 1H), 9.62 (br s, 1H), 11.82 (br s, 1H); MS-ESI m/z 334 ($M - H^+$).

(iii) 1-Isopropyl-3-[6-(trifluoromethoxy)benzothiazol-2-yl]thiourea (3c). Reflux for 54 h: white needles (23% yield); mp 242 °C; ^{1}H NMR (DMSO-d_6) δ 1.21 (d, 6H, J = 6.0), 4.33 (m, 1H), 7.33 (d, 1H, J = 8.6), 7.69 (d, 1H, J = 8.5), 7.99 (s, 1H), 9.36 (br s, 1H), 11.70 (br s, 1H); MS-ESI m/z 334 ($M - H^+$).

(iv) 1-Butyl-3-[6-(trifluoromethoxy)benzothiazol-2-yl]thiourea (3d). Reflux for 52 h: white needles (27% yield); mp 211 °C; ^{1}H NMR (DMSO-d_6) δ 0.88 (t, 3H, J = 7.2), 1.33 (m, 2H), 0.92 (m, 2H), 3.50 (m, 2H), 7.33 (d, 1H, J = 8.5), 7.66 (d, 1H, J = 8.5), 7.98 (s, 1H), 9.53 (br s, 1H), 11.80 (br s, 1H); MS-ESI m/z 348 ($M - H^+$).

(v) 1-Phenyl-3-[6-(trifluoromethoxy)benzothiazol-2-yl]thiourea (3e). Reflux for 30 h: white needles (22% yield); mp 234 °C; ^{1}H NMR (DMSO-d_6) δ 7.15 (m, 1H), 7.33 (m, 3H), 7.63 (m, 3H), 7.98 (s, 1H), 10.76 (br s, 2H); MS-ESI m/z 368 ($M - H^+$).

(vi) 1-(4-Fluorophenyl)-3-[6-(trifluoromethoxy)benzothiazol-2-yl]thiourea (3f). Reflux for 42 h: light-yellow needles (20%

yield); mp 207 °C; ^{1}H NMR (DMSO-d_6) δ 7.14 (m, 2H), 7.40 (m, 1H), 7.62 (m, 3H), 7.97 (s, 1H), 10.72 (br s, 2H); MS-ESI m/z 386 ($M - H^+$).

General Procedure for the Preparation of Guanidine Derivatives (4a,b). To a solution of the suitable thiourea (0.76 mmol) in acetone (40 mL) was added methyl iodide (0.84 mmol), and the mixture was stirred at room temperature under a nitrogen atmosphere. At the end of the reaction, the solvent was removed under reduced pressure, and the resulting residue was dissolved in ethanol and anhydrous ammonia bubbled for 20 min. The reaction flask was sealed, and the solution was stirred overnight. The solution was then concentrated in vacuo, and the residue was diluted with CH_2Cl_2 and washed with water. The combined organic layers were dried over Na_2SO_4, filtered, and concentrated in vacuo. The product was purified by flash chromatography using a petroleum ether/ethyl acetate (65:35, v/v) mixture as eluent. Recrystallization from *n*-hexane and diethyl ether gave the expected compound.

(i) 1-Ethyl-3-[6-(trifluoromethoxy)benzothiazol-2-yl]guanidine (4a). White pearly crystals (20% yield): mp 127−129 °C; ^{1}H NMR ($CDCl_3$) δ 1.27 (m, 3H), 3.28 (m, 2H), 6.28 (br s, 3H), 7.11 (d, 1H, $J = 8.9$), 7.24 (s, 1H), 7.47 (d, 1H, $J = 8.8$); MS-ESI m/z 305 ($M + H^+$).

(ii) 1-Propyl-3-[6-(trifluoromethoxy)benzothiazol-2-yl]guanidine (4b). White pearly crystals (22% yield): mp 110−111 °C; ^{1}H NMR ($CDCl_3$) δ 1.03 (t, 3H, $J = 7.4$), 1.70 (m, 2H), 3.19 (q, 2H, $J = 6.2$), 6.22 (br s, 3H), 7.11 (d, 1H, $J = 7.2$), 7.24 (s, 1H), 7.46 (d, 1H, $J = 8.8$); MS-ESI m/z 319 ($M + H^+$).

Neuroprotection Experiments. (i) Preparation of Animals and Slices. All experiments were performed in strict compliance with the recommendation of the EEC (86/609/CEE) for the care and use of laboratory animals, and the protocols were approved by the Animal Care and Ethics Committee of the University of Siena. Male Sprague-Dawley rats (350−450 g) (Charles River Italia, Calco, Italy) were sacrificed after anesthesia (ip injection of 30 mg of ketamine hydrocloride/kg of body weight and 8 mg of xylazine chloride/kg body weight), and the whole brains were rapidly removed and placed in aCSF (120 mM NaCl, 2.5 mM KCl, 1.3 mM $MgCl_2$, 1.0 mM NaH_2PO_4, 1.5 mM $CaCl_2$, 26 mM $NaHCO_3$, and 11 mM glucose, saturated with a 95% O_2/5% CO_2 mixture, with a final pH of 7.4, and osmolality of 285−290 mosM). The cortex was dissected and cut into 400 μm thick slices by using a manual chopper (Stoelting Co., Wood Dale, IL). Afterward, slices were maintained in oxygenated aCSF enriched with 400 μM ascorbic acid for 1 h at room temperature to allow maximal recovery from slicing trauma.[37]

(ii) In Vitro Ischemia-like Conditions. Cortical slices (≈4−5, total wet weight of 33.6 ± 2.6 mg, $n = 10$) were placed in covered incubation flasks, containing 2 mL of aCSF continuously bubbled with a 95% O_2/5% CO_2 mixture and incubated at 37 °C for an additional period of 30 min. Afterward, oxygen/glucose deprivation was conducted by incubating slices for 30 min in aCSF in which glucose was replaced with an equimolar amount of saccharose and continuously bubbled with a 95% N_2/5% CO_2 mixture. After the oxygen/glucose deprivation period, the ischemic solution was replaced with fresh, oxygenated aCSF for an additional 90 min (reoxygenation). In treated samples, oxygen/glucose deprivation was followed by reoxygenation with aCSF containing riluzole or the compounds under study.

(iii) Assessment of Neuronal Injury. Neuronal damage was assessed quantitatively by measuring the amount of both glutamate and LDH released into the aCSF during 90 min reoxygenation period. In particular, glutamate was measured fluorimetrically (excitation at 366 nm; emission at 450 nm) using the conversion of NAD^+ to NADH by glutamate dehydrogenase,[38] whereas LDH activity was determined spectrophotometrically by measuring the rate of the decrease in absorbance at 340 nm via the oxidation of NADH to NAD^+.[39]

(iv) Data Analysis. All the experiments were performed by using brain slices derived from at least four different rats. Data are reported as mean ± sem, and n is defined as the number of samples. For glutamate and LDH activity, data are expressed as nanomoles per milligram of tissue and units per milligram of tissue, respectively. One unit of LDH activity is defined as that which gives rise to 1 μmol of lactate/min.

Statistical analysis was performed by using one-way ANOVA followed by the post hoc Dunnett test (GraphPad INSTAT version 3.00, GraphPad Software, San Diego, CA).

Interaction of the Compounds with Nitric Oxide Synthase. The interactions of studied compounds with neuronal nitric oxide synthase were performed on rat brain partially purified preparations according to the method reported by Chen et al.[40] Briefly, rat brain homogenized in buffer (5 mL/g of tissue) containing (final concentrations) 320 mM sucrose, 20 mM HEPES [*N*-(2-hydroxyethyl)piperazine-*N*′-2-ehanesulfonic acid], 1 mM EDTA (ethylenediaminetetraacetic acid), 1 mM dithiothreitol, 10 μg/mL soybean trypsin inhibitor, and 10 mg/mL PMSF (phenylmethanesulfonyl fluoride) (pH 7.4) was centrifuged at 45000 rpm for 30 min and the supernatant collected. All procedures were performed at 4 °C. To remove endogenous L-arginine from the preparation, the supernatant was mixed with Dowex 50W (200−400 mesh 8% cross-linked) for 10 min and shaken. After that, the mixture was centrifuged at 9000 rpm for 5 min at 4 °C and the supernatant aliquoted out and kept at −80 °C until it was used. The protein content was determined according to the method of Lowry et al.[41]

Determination of nNOS Activity. The reaction was started by adding 0.02 mM L-arginine to the assay mixture [50 mM potassium phosphate buffer, pH 7.2 (final concentration) 1.15 μM oxyhemoglobin, 0.2 mM $CaCl_2$, 0.1 mM NADPH, and rat brain NOS preparations (2.0 mg/mL)] and followed by reading the change in absorbance versus time at 401 nm at the initial linear phase of the reaction.[30]

Oxyhemoglobin was purified from commercial hemoglobin (Sigma) by dissolving 20 mg in 1 mL of distilled water and adding sodium dithionite and oxygen over surface. Purification and desalting were carried out by eluting 300 μl of hemoglobin solution from a sephadex G-25 column (1 × 17 cm) using 1 M NaCl solution as eluent. The concentration of the hemoglobin was determined by measuring the absorbance at 415 nm ($\varepsilon = 131$ $mM^{-1} \times cm^{-1}$).

Antioxidant Activity. The antioxidant activities of the studied compounds were assayed by measuring spectrophotometrically the quenching of the stable cation radical $ABTS^{\cdot+}$ as reported by Re et al.[24] Briefly, the cation radical was obtained by reacting ABTS with ammonium persulfate (1:0.35) in a water solution for 24 h in the dark at room temperature. Further, the $ABTS^{\cdot+}$ solution diluted with ethanol to an absorbance value of 0.70 ± 0.02 at 751 nm was incubated in the presence of different concentrations (1−100 μM) of **3a**−**d** compounds or Trolox, as a reference compound. The decrease in absorbance at a λ of 751 nm was recorded 5 min after ABTS and compound(s) had been initially mixed and followed for 10 min. The data are reported as Trolox equivalent antioxidant capacity (TEAC). TEAC represents the ratio between the estimated concentration of the compound that promotes the decrease of radical cation $ABTS^{\bullet+}$ absorbance equal to 1 mM Trolox. The absorbance value for Trolox or compounds was estimated from the inhibition curve obtained by plotting the concentration versus absorbance (GraphPad Software) to determine the TEAC.

Patch-Clamp Experiments. Whole-cell, patch-clamp recordings were conducted in layer II pyramidal neurons of rat piriform cortex (PC), either in slices or after acute dissociation. Young (P15−P22) Wistar rats of either sex were used, following a protocol that conformed with the rules established by the University of Pavia for the use of animals in experimental studies, in compliance with the guidelines of the Italian Ministry of Health, the national laws on animal research (d.l. 116/92), and the EU guidelines on animal research (N. 86/609/CEE).

(i) Recordings of Voltage-Dependent Na^+ Currents from Neurons in Slices. The procedures followed and the solutions used for extracting and sectioning the brain were the same as those described previously.[42] The rostral part of the brain, containing the anterior piriform cortex, was glued on the stage of a vibratome, and 350 μm thick coronal sections were cut. The slices were kept submerged in the incubation chamber at room temperature for at least 1 h before the recording was begun.

The experimental apparatus employed and the recording procedures adopted for patch-clamp experiments in slices were also identical to those described elsewhere.[42] Slices were perfused with an extracellular solution suitable for the isolation of Na^+ currents and containing 100 mM NaCl, 26 mM $NaHCO_3$, 19.5 mM tetraethylammonium chloride (TEA-Cl), 3 mM KCl, 2 mM $MgCl_2$, 2 mM $CaCl_2$, 2 mM $BaCl_2$, 0.5 mM $CdCl_2$, 4 mM 4-aminopyridine (4-AP), and 11 mM D-glucose (pH 7.4 by saturation with a 95% O_2/5% CO_2 mixture). Patch pipettes were filled with an intracellular solution containing 104 mM CsF, 50 mM TEA-Cl, 2 mM $MgCl_2$, 10 mM *N*-(2-hydroxyethyl)piperazine-*N*′-2-ethanesulfonic acid (HEPES), 10 mM ethylene glycol bis(β-aminoethyl ether) *N*,*N*,*N*′,*N*′-tetraacetic acid (EGTA), 2 mM adenosine 5′-triphosphate (ATP)-Na_2, and 0.2 mM guanosine 5′-triphosphate (GTP)-Na (pH adjusted to 7.2 with CsOH).

The general holding potential of voltage-clamp recordings was −80 mV. Current signals were low-pass filtered and digitized at cutoff and sampling frequencies of 5 and 50 kHz, respectively. Currents were always online leak subtracted via a P/4 routine. Tetrodotoxin (TTx) (Alomone Laboratories, Jerusalem, Israel) was applied in the bath with the superfusing solution at the end of all recordings, and currents recorded in the presence of 1 μM TTx were always subtracted from those recorded under control conditions and in the presence of drugs to abolish residual, unsubtracted capacitive and/or leakage currents.

(ii) Recordings of Voltage-Dependent Ca^{2+} Currents from Acutely Dissociated Neurons. The procedures followed for extraction of the nervous tissue and dissection of PC layer II were described previously.[35] We acutely dispersed neurons by applying a mechanical and enzymatic dissociation procedure also described previously.[35]After being seeded in the recording chamber, cells were perfused with an oxygenated extracellular solution suitable for isolating Ba^{2+} currents conducted through Ca^{2+} channels, containing 88 mM choline-Cl, 40 mM TEA-Cl, 3 mM KCl, 2 mM $MgCl_2$, 5 mM $BaCl_2$, 3 mM CsCl, 10 mM HEPES, 5 mM 4-AP, and 25 mM D-glucose (pH 7.4 with HCl). Patch pipettes were filled with an intracellular solution containing 78 mM Cs methanesulfonate, 40 mM TEA-Cl, 10 mM HEPES, 10 mM EGTA, 20 mM phosphocreatine di-Tris salt, 2 mM ATP-Na_2, and 20 units/mL creatine phosphokinase (pH adjusted to 7.2 with CsOH). Tight seals (> 5 GΩ) and the whole-cell configuration were obtained according to the standard technique.[33] All recording conditions were as previously described.[35]

The general holding potential of voltage-clamp recordings was −70 mV. Either step or ramp protocols were commanded to activate voltage-dependent Ca^{2+} currents. In both cases, a 2 s conditioning prepulse at −60 mV preceded each test depolarization. Current signals were filtered at 5 kHz and digitized at 50 kHz. Step protocols were online leak subtracted via a P/4 protocol.

(iii) Drug Application. Concentrated (30 mM) stock solutions of riluzole and compounds **3b** and **3d** were prepared in DMSO, divided into small aliquots, and stored at −20 °C. The aliquots were then diluted to the final concentrations in one of the extracellular solutions described above. Because an insoluble precipitate formed when **3b** and **3d** stocks were dissolved in this solution at high concentrations (60−200 μM), **3b**- and **3d**-containing solutions were always filtered before application. Preliminary control experiments indicated that DMSO had no significant effects on Ca^{2+} currents when applied at the same concentrations used to dissolve drugs in aqueous solution (0.02−0.67%, v/v).

In experiments for recording Na^+ currents in slices, the drug-containing extracellular solution was applied through the bath perfusion. In experiments for recording Ca^{2+} currents in acutely dissociated neurons, drugs were applied through a local-perfusion system consisting of a multibarrel pipet (diameter at the tip of ~150 μm), each barrel of which was connected to a separate perfusion channel. When each channel was opened, controlled by operation of on remote-commanded electrovalves (Sirai, Milano, Italy), the drug-containing solution flowed by gravity, thus forming a laminar-flux cone. The tip of the perfusion pipet was positioned in the proximity of the recording site, so that the recorded cell was fully drenched by the laminar-flux cone.

(iv) Data Analysis. Whole-cell current signals were analyzed using Clampfit from pClamp version 8.2 (Axon Instruments, Union City, CA). Na^+ currents were normally refiltered off-line at 3.5 kHz. Current amplitude was measured at the peak of each tracing. Current−voltage (I/V) plots for I_{Ba} were fitted by applying the following function, which is a combination of the Boltzmann function and the Goldman equation:

$$\begin{aligned} I_{Ba} &= (P_{Ba(max)}/\{1+\exp[(V_m - V_{1/2})/k]\}) \\ &\times (4F^2V_m)/(RT) \\ &\times \{[Ba^{2+}]_i - [Ba^{2+}]_o \\ &\times \exp[(-2FV_m)/(RT)]\}/\{1-\exp[(-2FV_m)/(RT)]\} \end{aligned} \quad (1)$$

in which the nominal intra- and extracellular Ba^{2+} concentration values (0 and 5 mM, respectively) were introduced and where $P_{Ba(max)}$ is the maximal Ba^{2+} permeability, V_m is the membrane potential, $V_{1/2}$ and k are the half-maximal activation potential and slope factor, respectively, of the Boltzmann activation function, and F, R, and T have their usual meanings.

Tail-current decay could be consistently best fitted with a second-order exponential function:

$$I = A_1 \times \exp(-t/\tau_{d1}) + A_2 \times \exp(-t/\tau_{d2}) + C \quad (2)$$

Because at relatively positive repolarization potentials the slower exponential component could be influenced by channel inactivation, the analysis was focused on the faster deactivation time constant (τ_{d1}). Since the importance of τ_{d1} in governing the deactivation process is determined not only by its value but also by its relative weight, to obtain an overall description of the fast component of tail current decay we calculated the following parameter:

$$\bar{\tau}_{d1} = \tau_{d1}/[A_1/(A_1+A_2)] \quad (3)$$

namely, the fast time constant divided by its relative amplitude. Hence, the lower τ_{d1} is and the higher its relative weight, the smaller $\bar{\tau}_{d1}$, which represents a "weighted" version of the fast deactivation time constant.

Data fittings with eqs 1 and 2 were conducted using Origin version 6.0 (MicroCal Software, Northampton, MA) and Clampfit version 8.2, respectively.

Average values were expressed as arithmetic means ± sem. Statistical significance was evaluated by applying the two-tail Student's t test for paired or unpaired data.

Acknowledgment. We thank Rottapharm SpA (Monza, Italy) for financial support of this research and Prof. Stefania D'Agata D'Ottavi for the careful reading of the manuscript. This work has been performed with the financial support of the University of Siena, Piano di Ateneo per la Ricerca (PAR) 2006.

Supporting Information Available: Microanalytical data of compounds **2**−**4**. This material is available free of charge via the Internet at http://pubs.acs.org.

References

(1) Dong, X. X.; Wang, Y.; Qin, Z. H. Molecular mechanisms of excitotoxicity and their relevance to pathogenesis of neurodegenerative diseases. *Acta Pharmacol. Sin.* **2009**, *30*, 379–387.

(2) Besancon, E.; Guo, S.; Lok, J.; Tymianski, M.; Lo, E. H. Beyond NMDA and AMPA glutamate receptors: Emerging mechanisms for ionic imbalance and cell death in stroke. *Trends Pharmacol. Sci.* **2008**, *29*, 268–275.

(3) Brown, G. C. Mechanisms of inflammatory neurodegeneration: *i*NOS and NADPH oxidase. *Biochem. Soc. Trans.* **2007**, *35*, 1119–1121.

(4) Nicholls, D. G. Mitochondrial dysfunction and glutamate excitotoxicity studied in primary neuronal cultures. *Curr. Mol. Med.* **2004**, *4*, 149–177.

(5) Fernandez-Espejo, E. Pathogenesis of Parkinson's disease: Prospects of neuroprotective and restorative therapies. *Mol. Neurobiol.* **2004**, *29*, 15–30.

(6) Bonelli, R. M.; Wenning, G. K.; Kapfhammer, H. P. Huntington's disease: Present treatments and future therapeutic modalities. *Int. Clin. Psychopharmacol.* **2004**, *19*, 51–62.

(7) Ates, O.; Cayli, S. R.; Gurses, I.; Karabulut, A. B.; Yucel, N.; Kocak, A.; Cakir, C. O.; Yologlu, S. Do sodium channel blockers have neuroprotective effect after onset of ischemic insult? *Neurol. Res.* **2007**, *29*, 317–323.

(8) Bensimon, G.; Lacomblez, L.; Meininger, V. A controlled trial of riluzole in amyotrophic lateral sclerosis. ALS/Riluzole study group. *N. Engl. J. Med.* **1994**, *330*, 585–591.

(9) Bryson, H. M.; Fulton, B.; Benfield, P. Riluzole: A review of its pharmacodynamic and pharmacokinetic properties and therapeutic potential in amyotrophic lateral sclerosis. *Drug Eval.* **1996**, *52*, 549–563.

(10) Miller, R. G.; Mitchell, J. D.; Lyon, M.; Moore, D. H. Riluzole for amyotrophic lateral sclerosis (ALS)/motor neuron disease (MND). *Cochrane Database Syst. Rev. 2* **2002**, CD001447.

(11) Benoit, E.; Escande, D. Riluzole specifically blocks inactivated Na channels in myelinated nerve fibre. *Pfluegers Arch.* **1991**, *419*, 603–609.

(12) Hebert, T.; Drapeau, P.; Pradier, L.; Dunn, R. J. Block of the rat brain IIA sodium channel α subunit by the neuroprotective drug riluzole. *Mol. Pharmacol.* **1994**, *45*, 1055–1060.

(13) Song, J. H.; Huang, C. S.; Nagata, K.; Yeh, J. Z.; Narahashi, T. Differential action of riluzole on tetrodotoxin-sensitive and tetrodotoxin-resistant sodium channels. *J. Pharmacol. Exp. Ther.* **1997**, *282*, 707–714.

(14) Zona, C.; Siniscalchi, A.; Mercuri, N. B.; Bernardi, G. Riluzole interacts with voltage-activated sodium and potassium currents in cultured rat cortical neurons. *Neuroscience* **1998**, *85*, 931–938.

(15) Debono, M. W.; Le Guern, J.; Canton, T.; Doble, A.; Pradier, L. Inhibition by riluzole of electrophysiological responses mediated by rat kainate and NMDA receptors expressed in *Xenopus* oocytes. *Eur. J. Pharmacol.* **1993**, *235*, 283–289.

(16) Doble, A. The pharmacology and mechanism of action of riluzole. *Neurology* **1996**, *47* (Suppl. 4), S233–S241.

(17) Martin, D.; Thompson, M. A.; Nadler, J. V. The neuroprotective agent riluzole inhibits release of glutamate and aspartate from slices of hippocampal area CA1. *Eur. J. Pharmacol.* **1993**, *250*, 473–476.

(18) Frizzo, M. E.; Dall'Onder, L. P.; Dalcin, K. B.; Souza, D. O. Riluzole enhances glutamate uptake in rat astrocyte cultures. *Cell. Mol. Neurobiol.* **2004**, *24*, 123–128.

(19) Ginsberg, M. D. Neuroprotection for ischemic stroke: Past, present and future. *Neuropharmacology* **2008**, *55*, 363–389.

(20) Zhu, Y.; Nikolic, D.; Van Breemen, R. B.; Silverman, R. B. Mechanism of inactivation of inducible nitric oxide synthase by amidines. Irreversible enzyme inactivation without inactivator modification. *J. Am. Chem. Soc.* **2005**, *127*, 858–868.

(21) Iravani, M. M.; Liu, L.; Rose, S.; Jenner, P. Role of inducible nitric oxide synthase in N-methyl-D-aspartic acid-induced strio-nigral degeneration. *Brain Res.* **2004**, *1029*, 103–113.

(22) Babbedge, R. C.; Hart, S. L.; Moore, P. K. Anti-nociceptive activity of nitric oxide synthase inhibitors in the mouse: Dissociation between the effect of L-NAME and L-NMMA. *J. Pharm. Pharmacol.* **1993**, *45*, 77–79.

(23) Kim, S. G.; Kim, H. J.; Yang, C. H. Thioureas differentially induce rat hepatic microsomal epoxide hydrolase and rGSTA2 irrespective of their oxygen radical scavenging effect: Effects on toxicant-induced liver injury. *Chem.-Biol. Interact.* **1999**, *117*, 117–134.

(24) Re, R.; Pellegrini, N.; Proteggente, A.; Pannala, A.; Yang, M.; Rice-Evans, C. Antioxidant activity applying an improved ABTS radical cation decolorization assay. *Free Radical Biol. Med.* **1999**, *26*, 1231–1237.

(25) Jordan, A. D.; Luo, C.; Reitz, A. B. Efficient conversion of substituted aryl thioureas to 2-aminobenzothiazoles using benzyltrimethylammonium tribromide. *J. Org. Chem.* **2003**, *68*, 8693–8696.

(26) Farkas, L.; Kasztreiner, E.; Andrasi, F.; Borsi, J.; Kosary, J.; Csanyi, E.; Elek, S. Thiazolylurea derivatives and process for the preparation thereof. Patent GB 1437895, 1976-06-03. EC: C07D417/04; C07D417/14.

(27) Latli, B.; D'Amour, K.; Casida, J. E. Novel and potent 6-chloro-3-pyridinyl ligands for the α4β2 neuronal nicotinic acetylcholine receptor. *J. Med. Chem.* **1999**, *42*, 2227–2234.

(28) Doyle, K. P.; Simon, R. P.; Stenzel-Poore, M. P. Mechanisms of ischemic brain damage. *Neuropharmacology* **2008**, *55*, 310–318.

(29) Chen, Q. M.; LaBella, F. S. Inhibition of nitric oxide synthase by straight chain and cyclic alcohols. *Eur. J. Pharmacol.* **1997**, *321*, 355–360.

(30) Salter, M.; Knowels, G. R. Assay of NOS activity by the measurement of conversion of oxyhemoglobin to methemoglobin by NO. *Methods in Molecular Biology*; Nitric Oxide Protocols; Titheradge, M. A., Ed.; Humana Press: Totowa, NJ, 1998; Vol. 100, Chapter 6, pp 61−66.

(31) Satoh, T.; Ishige, K.; Sagara, Y. Protective effects on neuronal cells of mouse afforded by ebselen against oxidative stress at multiple steps. *Neurosci. Lett.* **2004**, *371*, 1–5.

(32) Huang, C. S.; Song, J. H.; Nagata, K.; Yeh, J. Z.; Narahashi, T. Effects of the neuroprotective agent riluzole on the high voltage-activated calcium channels of rat dorsal root ganglion neurons. *J. Pharmacol. Exp. Ther.* **1997**, *282*, 1280–1290.

(33) Hamill, O. P.; Marty, A.; Neher, E.; Sakmann, B.; Sigworth, F. J. Improved patch-clamp techniques for high-resolution current recording from cells and cell-free membrane patches. *Pfluegers Arch.* **1981**, *391*, 85–100.

(34) Castelli, L.; Nigro, M. J.; Magistretti, J. Analysis of resurgent sodium-current expression in rat parahippocampal cortices and hippocampal formation. *Brain Res.* **2007**, *1163*, 44–55.

(35) Magistretti, J.; Castelli, L.; Taglietti, V.; Tanzi, F. Dual effect of Zn^{2+} on multiple types of voltage-dependent Ca^{2+} currents in rat palaeocortical neurons. *Neuroscience* **2003**, *117*, 249–264.

(36) Jimonet, P.; Audiau, F.; Barreau, M.; Blanchard, J.-C.; Boireau, A.; Bour, Y.; Coleno, M. A.; Doble, A.; Doerflinger, G.; Do Huu, C.; Donat, M. H.; Duchesne, J. M.; Ganil, P.; Gueremy, C.; Honore, E.; Just, B.; Kerphirique, R.; Gontier, S.; Hubert, P.; Laduron, P. M.; Le Blevec, J.; Meunier, M.; Miquet, J. M.; Nemecek, C.; Pasquet, M.; Piot, O.; Pratt, J.; Rataud, J.; Reibaud, M.; Stutzmann, J. M.; Mignani, S. Riluzole series. Synthesis and *in vivo* "antiglutamate" activity of 6-substituted-2-benzothiazolamines and 3-substituted-2-imino-benzothiazolines. *J. Med. Chem.* **1999**, *42*, 2828–2843.

(37) Brahma, B.; Forman, R. E.; Stewart, E. E.; Nicholson, C.; Rice, M. E. Ascorbate inhibits edema in brain slices. *J. Neurochem.* **2000**, *74*, 1263–1270.

(38) Eilers, H.; Kindler, C. H.; Bickler, P. E. Different effects of volatile anesthetics and polyhalogenated alkanes on depolarization-evoked glutamate release in rat cortical brain slices. *Anesth. Analg.* (*Hagerstown, MD, U.S.*) **1999**, *88*, 1168–1174.

(39) Gay, R. J.; McComb, R. B.; Bowers, G. N., Jr. Optimum reaction conditions for human lactate dehydrogenase isoenzymes as they affect total lactate dehydrogenase activity. *Clin. Chem.* **1968**, *14*, 740–753.

(40) Chen, Q. M.; LaBella, F. S. Inhibition of nitric oxide synthase by straight chain and cyclic alcohols. *Eur. J. Pharmacol.* **1997**, *321*, 355–360.

(41) Lowry, O. H.; Rosebrough, N. J.; Farr, A. L.; Randall, R. J. Protein measurement with the Folin phenol reagent. *J. Biol. Chem.* **1951**, *193*, 265.

(42) Magistretti, J.; Castelli, L.; Forti, L.; D'Angelo, E. Kinetic and functional analysis of transient, persistent, and resurgent sodium currents in rat cerebellar granule cells *in situ*: An electrophysiological and modeling study. *J. Physiol.* **2006**, *573*, 83–106.